Fast Iterative Poisson Solver for Molecular Junctions' Geometries†

Oded Godsi, Ilan Bar-On, and Uri Peskin*

Department of Chemistry and The Lise Meitner Center for Computational Quantum Chemistry, Technion-Israel Institute of Technology, Haifa 32000, Israel

Received: March 6, 2003

A new numerical method is introduced for the solution of Poisson's equation for the electrostatic potential between arbitrarily shaped boundary surfaces that may appear in metal−molecule−metal junctions. This method is based on a straightforward procedure in which the arbitrarily shaped system is embedded in a cubic box. The embedding procedure is formulated in terms of boundary operators that can be readily implemented even for complex irregular geometries of the boundary surfaces. The solution to Poisson's equation on a cubic mesh (i.e., the inverse Laplacian operation) is used as a preconditioner, and the solution of the noncubic, more complex electrostatic problem is obtained by an error-minimization scheme that is based on a Krylov subspace expansion method. The accuracy and fast convergence of this numerical procedure are demonstrated for generic examples.

1. Introduction

The recent experimental measurements of electron transport through (single) molecules between two electrodes (a molecular junction) under an electrostatic potential bias[1−8] introduce new challenges to quantum chemical calculations and to quantum dynamics simulations. The main difficulty in the theoretical modeling of a molecular junction is associated with the unique boundary conditions due to the (strong) coupling of the molecule to the continuum of states in the metal electrodes. Under these conditions, the many-body system is open, and neither periodic boundary conditions nor reflecting boundary conditions (as applied in basis set expansions) are rigorously appropriate. It is therefore common to focus on the molecule under study (perhaps with a few additional metal atoms) and to apply boundary conditions that introduce the effect of the "external" metal electrodes.[9−16] The latter are typically at different electrostatic potentials, and their shape can be quite general.

The charge distribution $\rho(x, y, z)$ inside a junction is related to the electrostatic potential $\Phi(x, y, z)$ by the Poisson equation,

$$\hat{\Delta}\Phi(x, y, z) = -4\pi\rho(x, y, z) \tag{1.1}$$

When all of the charges in the system (including electrons and nuclei (or atomic cores)) are treated explicitly, the solution to the Poisson equation is the well-known Coulomb integral,

$$\Phi(x, y, z) = \int\int\int \frac{\rho(x', y', z')\, dx'\, dy'\, dz}{\sqrt{(x - x')^2 + (y - y')^2 + (z - z')^2}}$$

In fact, numerical solutions of Poisson's equation provide an efficient tool for evaluating such Coulomb integrals in quantum chemistry applications.[17] However, the charges in the semi-infinite metal electrodes cannot be accounted for explicitly. Rather, they impose the appropriate boundary conditions on the open molecular junctions, particularly the externally applied voltage bias.[18−23] It is therefore anticipated that the solution of Poisson's equation for general boundary surfaces (in terms of their shape and electrostatic potential) would become useful in the study of electronic transport in molecular junctions. Motivated by this ongoing development, we introduce in this paper a new numerical approach for the solution of the relevant electrostatic boundary value problem.

The numerical solution of Poisson's equation on regular domains (i.e., rectanglar in 2D and cubic in 3D) is well known, and numerous algorithms exist for its solution. Fast direct solvers[24,25] employing Fourier transform[26,27] and cyclic reduction methods[28,29] are some examples. However, their generalization to irregular domains of a general boundary shape, as in our cases of interest, is not straightforward. There are basically two approaches to this problem.[30]

One approach is to subdivide the irregular region into smaller regions of regular shapes and then apply a domain decomposition solver to the whole system of subdomains. This would be the method of choice when applied to an ensemble of objects with natural boundaries. However, the implementation involves several stages (i.e., separate discretizations in terms of finite difference[31] or finite element[32] methods, a multigrid solver,[33] a domain decomposition algorithm,[34] and a Krylov subspace accelerator[35,36]).

The other option, which is more appropriate in the present cases of interest where there are no natural subboundaries, is to embed the irregular region inside a regular (e.g., cubic) region for which the solution is found directly as above. In this approach, the values of the electrostatic potential on the irregular boundaries are replaced with equivalent charge distributions (the irregular boundaries are internal to the domain) using the capacitance matrix method.[37,38] However, the method becomes computationally intensive as the number of grid points on the irregular boundaries grows. A more recently suggested method for this problem is the boundary integral method.[39]

In this work, we propose a novel embedding method that is much simpler to implement and works efficiently in practice on general irregular domains. Our strategy is to incorporate the boundary conditions as additions to the Laplacian operator (matrix) and then use the direct solver on the regular domain

† Part of the special issue "Donald J. Kouri Festschrift".

* Corresponding author. E-mail: uri@chem.technion.ac.il.

10.1021/jp030308n CCC: $25.00
Published on Web 07/03/2003

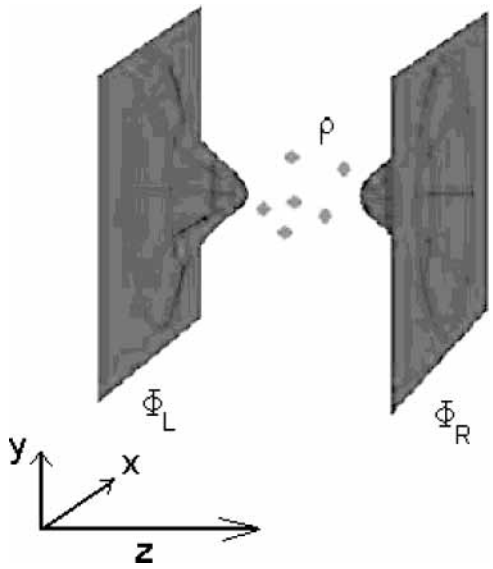

Figure 1. Schematic illustration of the charge distribution ρ between two electrode surfaces.

as a preconditioner. To accelerate (and ensure) convergence, we employ a Krylov subspace solver such as the quasiminimal residual (QMR) algorithm.[40−42] Thus, the method amounts to the use of a separable preconditioner within a Krylov subspace accelerator. Separable preconditioners that are based on the inverse of a separable differential operator (the Laplacian on a rectangular mesh, in the present case) with periodic boundary conditions were suggested before[43−51] in iterative solutions of the inhomogeneous Schrödinger and Helmholtz equations. For the Poisson equation, it was recently demonstrated that the same numerical approach can be applied when the asymptotic solution (i.e., the electrostatic potential) can be approximated analytically, such as for a solute in a nonuniform dielectric medium.[52]

In the following section, we reformulate the Poisson equation with specific boundary surfaces as an inhomogeneous linear system in a 3D cubic domain using boundary operators. The preconditioner is introduced in section 3, and numerical examples in which the electrostatic potential is calculated for generic illustrative models are reported in section 4. Concluding remarks and a discussion are given in section 5.

2. Poisson Equation with Boundary Operators

We consider the Poisson equation (eq 1.1) in three dimensions, where $\rho(x, y, z)$ is a given electric charge density. We assume that the electrostatic potential $\Phi(x, y, z)$ is defined at some boundary surfaces, surrounding a volume in which it is unknown. Focusing on electrode−conductor−electrode systems as illustrated in Figure 1, two boundary surfaces representing the electrodes are characterized by known constant values of the electrostatic potentials. Let us define the axis in the perpendicular direction to the two electrode surfaces as the z axis. The boundary conditions are therefore

$$\Phi[x, y, z_R(x, y)] = \Phi_R[x, y, z_R(x, y)]$$
$$\Phi[x, y, z_L(x, y)] = \Phi_L[x, y, z_L(x, y)] \quad (2.1)$$

where $z_R(x, y)$ and $z_L(x, y)$ are the right and left boundary surfaces, respectively, and the corresponding electrostatic potentials are $\Phi_R[x, y, z_R(x, y)]$ and $\Phi_L[x, y, z_L(x, y)]$.

Our purpose here is to reformulate the Poisson equation such that the boundary conditions will be imposed explicitly on the solution *within a cubic (regular) box*. To achieve that, we introduce appropriate changes to the right-hand side of the equation as well as to the differential operator. We rewrite eq 1.1 as follows:

$$[\hat{\Delta} + \hat{B}]\Phi(x, y, z) = b(x, y, z) \quad (2.2)$$

The right-hand function includes the charge distribution as well as boundary terms (in the present case,two boundary surfaces):

$$b(x, y, z) = -4\pi\rho(x, y, z) + b_R(x, y, z) + b_L(x, y, z) \quad (2.3)$$

The terms $b_R(x, y, z)$ and $b_L(x, y, z)$ represent the electrodes. In agreement with eq 1.1, they vanish in the volume between the electrodes. At the boundaries, they are taken to be equal to the corresponding boundary electrostatic potentials (eq 2.1), and in the interior volume of each electrode (i.e., for $z > z_R(x, y)$ or $z < z_L(x, y)$), they can be assigned arbitrary values because the physically relevant solution between the electrodes is uniquely defined by the charge distribution and by the electrostatic potential at the boundaries. These interior volumes of the electrodes are artificially embedded in a cubic grid. The boundary terms are therefore defined as

$$b_R(x, y, z) = h(x, y, z - z_R(x, y))\Phi_R(x, y, z) \quad (2.4a)$$

$$b_L(x, y, z) = [1 - h(x, y, z - z_L(x, y))]\Phi_L(x, y, z) \quad (2.4b)$$

where $h(x, y, z)$ is a step function along the z direction:

$$h(x, y, z) = \begin{cases} 1 & z \geq 0 \\ 0 & z < 0 \end{cases} \quad (2.5)$$

The corresponding addition to the differential operator in eq 2.2 is introduced to impose the boundary values explicitly on the solution. Formally, we define the boundary operator $\hat{B}$ as

$$\hat{B} = [h(x, y, z - z_R(x, y)) + 1 - h(x, y, z - z_L(x, y))][\hat{I} - \hat{\Delta}] \quad (2.6)$$

Substituting eqs 2.3−2.6 into eq 2.2 results in an inhomogeneous equation that is identical to eq 1.1 for the interior points between the electrodes and explicitly imposes the appropriate electrostatic potentials at the boundaries.

The left-hand operator, $\hat{B} + \hat{\Delta}$, in the inhomogeneous eq 2.2 is sparse in a spatially discrete grid representation, as explained below. Therefore, the equation is suitable for an iterative solution using Krylov subspace-based methods. The operator can be divided into three terms. The first is the Laplacian operator, $\hat{\Delta} = \nabla_x^2 + \nabla_y^2 + \nabla_z^2$, which is separable in the three coordinates; therefore, its discrete matrix representation is sparse even when high-order finite difference methods are applied.[49] (For N grid points in each spatial dimension, the size of the matrix is $(N^3)^2$, but there are at most $3N^4$ nonzero entries.) The second term (eq 2.6) is $[h(x, y, z - z_R(x, y)) + 1 - h(x, y, z - z_L(x, y))]\hat{I}$, which is diagonal in the spatial grid representation. The third term, $[h(x, y, z - z_R(x, y)) + 1 - h(x, y, z - z_L(x, y))]\hat{\Delta}$, is a sequence (a successive operation) of the sparse Laplacian matrix and the diagonal matrix. The approximate solution (of order k) to eq 2.2 in a Krylov subspace, $K_{k+1}(\hat{B} + \hat{\Delta}, b)$, reads

$$\Phi_k(x, y, z) = \sum_{l=0}^{k} \alpha_l[\hat{B} + \hat{\Delta}]^l b(x, y, z) \quad (2.7)$$

where the expansion coefficients $\{\alpha_l\}$ can be optimized by an appropriate error-minimization criterion. It is important to point out that the matrix representation of the left-hand operator $\hat{B} + \hat{\Delta}$ in eq 2.2 is a real nonsymmetric matrix; therefore, the

resulting linear system is non-Hermitian. An appropriate residual-minimization algorithm for such systems is the transpose-free quasi-minimal residual (TFQMR) algorithm of Freund and Nachtigal.[40−42]

3. Separable Preconditioner

A crucial step in our scheme is the choice of an appropriate preconditioner. A useful approach is to apply an approximate inverse of the differential operator as a preconditioner. In some recent applications,[43−49] the separable part of the differential operator was chosen for this purpose. Here we use the separability of the Laplacian on the cubic mesh and apply the same strategy. Consider a separable differential operator, $\hat{S}$, in a 3D coordinate space,(x, y, z), such that $\hat{S} \equiv \hat{S}_x + \hat{S}_y + \hat{S}_z$. Although the matrix representation of $\hat{S}$ is sparse in any spatially discrete grid representation, the inverse matrix is not sparse. However, the inverse matrix can be applied as a sequence of sparse matrix multiplications using the diagonalization transformation $S^{-1} = \mathbf{U}\boldsymbol{\lambda}^{-1}\mathbf{U}^{-1}$. $\mathbf{U}$ is a sequence of sparse matrices for any separable $\hat{S}$ because $\mathbf{U} = U_x \otimes U_y \otimes U_z$ where $S_xU_x = U_x\lambda_x$, $S_yU_y = U_y\lambda_y$, and $S_zU_z = U_z\lambda_z$. $\boldsymbol{\lambda}$ is a diagonal matrix whose elements are given by $\boldsymbol{\lambda} = \lambda_x \otimes I_y \otimes I_z + I_x \otimes \lambda_y \otimes I_z + I_x \otimes I_y \otimes \lambda_z$.

In the present case, the preconditioner is the inverse of the Laplacian operator, $\hat{\Delta} = \nabla_x^2 + \nabla_y^2 + \nabla_z^2$. Invoking periodic boundary conditions on the rectangular mesh, the eigenvector matrix transformation $\mathbf{U} = U_x \otimes U_y \otimes U_z$ amounts to the 3D Fourier transform (the Fourier grid preconditioner[43]). (Recently, a similar approach was applied in solving the Poison equation in a nonuniform dielectric medium,[52] which was reformulated as a Helmholtz equation with an analytically approximated asymptotic potential.) The spectrum of the Laplacian operator includes the zero eigenvalue. This singularity can be easily removed by shifting the operator by an appropriate scalar constant[43] so that eq 2.2 can be rewritten as

$$[\hat{\Delta} + c - c + \hat{B}]\Phi(x, y, z) = b(x, y, z) \tag{3.1}$$

Applying the inverse of $[\hat{\Delta} + c]$ to both sides of eq 3.1, we obtain the preconditioned linear system

$$[\hat{I} + (\hat{\Delta} + c)^{-1}(\hat{B} - c)]\Phi(x, y, z) = [\hat{\Delta} + c]^{-1}b(x, y, z) \tag{3.2}$$

By analogy to eq 2.7, the approximate solution can be expanded in the corresponding Krylov subspace, $K_{k+1}([\hat{I} + (\hat{\Delta} + c)^{-1}(\hat{B} - c)], (\hat{\Delta} + c)^{-1}b)$, as follows:

$$\Phi^{(k)}(x, y, z) = \sum_{l=0}^{k} \beta_l [\hat{I} + (\hat{\Delta} + c)^{-1}(\hat{B} - c)]^l [\hat{\Delta} + c]^{-1} b(x, y, z) \tag{3.3}$$

The coefficients$\{\beta_l\}$ are optimized by an error-minimization scheme.

4. Numerical Implementation

In the examples below, we demonstrate calculations of the electrostatic potential for model systems in which charge points are positioned between two surfaces at constant electrostatic potentials. Two cases are considered. In the first case, the metal plates are taken to be flat and parallel to each other. In this case, the electrostatic potential can be calculated analytically in terms of an infinite summation over image charges potentials, which represent the metallic surfaces.[53] This calculation can therefore be used to analyze the accuracy and convergence properties of the proposed solver. In the second calculation, we consider nonflat tip-shaped electrodes.

TABLE 1: Numerical Grid Parameters[a]

	Δ_x	Δ_y	Δ_z	N_x	N_y	N_z
Figure 2	0.1	0.1	0.035	100	100	160
Figure 3	0.1	0.1	0.035	40, 60, 100	40, 60, 100	160
Figure 4	0.2	0.2	0.2	60	60	100
Figure 5	0.2	0.2	0.2	60	60	100
Figure 6	0.2	0.2	0.2	60	60	100

[a] Distances are in au.

The systems were modeled in a cubic box in which the Cartesian coordinates were discretized on an equally spaced mesh defined as

$$x_i = x_0 + (i - 1)\Delta_x \qquad i = 1, 2, ..., N_x \tag{4.1.a}$$

$$y_j = y_0 + (j - 1)\Delta_y \qquad j = 1, 2, ..., N_y \tag{4.1.b}$$

$$z_k = z_0 + (k - 1)\Delta_z \qquad k = 1, 2, ..., N_z \tag{4.1.c}$$

The numerical values of these grid parameters for the different calculations are summarized in Table 1. The inverse Laplacian operator was applied as a preconditioner using the discrete Fourier transform

$$[\Delta + c]^{-1} = \mathbf{F}^{-1}[c - \boldsymbol{\lambda}]^{-1}\mathbf{F} \tag{4.2}$$

where the operation $\mathbf{F}$ was implemented using the fast Fourier transform (FFT) algorithm with a complexity of $O(N \log(N))$ operation ($N = N_xN_yN_z$) and $\boldsymbol{\lambda}$ is the diagonal eigenvalues matrix, whose nonzero elements are

$$\lambda_{i,j,k} = \left[\frac{-N_x\pi + 2\pi(i-1)}{N_x\Delta_x}\right]^2 + \left[\frac{-N_y\pi + 2\pi(j-1)}{N_y\Delta_y}\right]^2 + \left[\frac{-N_z\pi + 2\pi(k-1)}{N_z\Delta_z}\right]^2 \tag{4.3}$$

for $i = 1, 2, ..., N_x$; $j = 1, 2, ..., N_y$; and $k = 1, 2, ..., N_z$.

In the first model, the two boundary surfaces representing the electrodes (eq 2.1) were taken to be parallel and flat:

$$z_R(x, y) = \frac{Z_0}{2} \qquad z_L(x, y) = -\frac{Z_0}{2} \tag{4.4}$$

The distance between the electrodes was taken to be $Z_0 = 5.4$ au, and the electrostatic potential at the two electrodes was taken to be zero:

$$\Phi_L[x, y, z_L(x, y)] = \Phi_R[x, y, z_R(x, y)] = 0 \tag{4.5}$$

In the lateral directions (x and y), periodic boundary conditions were applied, corresponding to periodic replications of the charges, where the four nearest neighbors of each charge are positioned at distances of $\pm\Delta_xN_x$ in the x direction and $\pm\Delta_yN_y$ in the y direction. Choosing the lateral boundaries of the cubic box sufficiently far from the charges ensures that the periodic model closely approximates the model of a single charge distribution. We emphasize that the problem of flat parallel electrodes is particularly simple because it has a formal analytic solution. The proposed numerical method was applied for this test case to demonstrate its feasibility. The system was embedded in a box, which is larger than the volume between the electrodes, and parts of the two electrodes were included explicitly in the model in terms of the boundary operators.

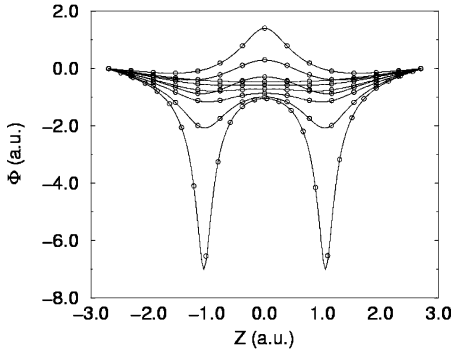

Figure 2. Comparison between the numerical (○) and analytical (—) solutions of Poisson's equation for the charge distribution between two flat electrodes. The different curves correspond to different choices of fixed lateral (x, y) coordinates, [(−1, −1), (−0.8, −0.8), (−0.6, −0.6), ..., (0.8, 0.8), (1, 1)] all in au. The numerical grid parameters are given in Table 1.

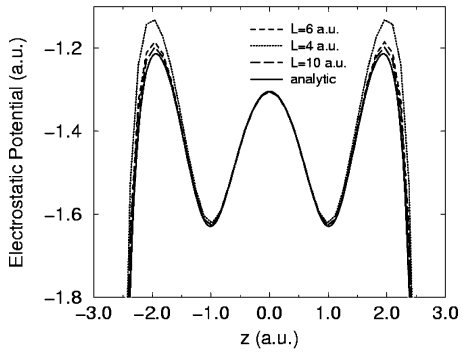

Figure 3. Electrostatic potential for a negative charge in a system of two positive charges between two flat electrodes. The solid line is an analytical result obtained by the method of images, and the long-dashed, dashed, and dotted lines are numerical results obtained for different values of lateral box length L. The numerical grid parameters are given in Table 1.

In the first test case, three charges were positioned on grid points between the electrodes. Two positive (proton) charges were located at points (0, 0, −1.05) and (0, 0, 1.05) au, and a negative (electron) charge was located at point (1, 1, 0). The Poisson equation was solved according to eqs 3.2 and 3.3 using the transpose-free quasi-minimal residual algorithm.[40−42] The numerical grid parameters are reported in Table 1. In Figure 2, the solution $\Phi(x, y, z)$ is plotted as a function of z for various sets of (x, y) values, illustrating the modulation of the z dependence of $\Phi(x, y, z)$ for different distances from the point charges. The numerical values are compared to analytical results, calculated by the method of images with the appropriate lateral periodic boundary conditions. These results demonstrate the accuracy of the numerical solution.

As a second test, we calculated the electrostatic potential for a simplistic and yet generic model in which two static proton charges were positioned between the two flat, ideal metallic electrodes. The two charges were located at points (0, 0, −1.05) and (0, 0, 1.05) au, and the plates were positioned as before at $z = \pm 2.7$ au. In Figure 3, numerically and analytically calculated results are plotted. The plots illustrate the z dependence of the electrostatic potential for fixed values $x = 0.5$ and $y = 0.5$ au. The potential at each point was defined as the solution to Poisson's equation as a boundary value problem (eq 3.2) with an additional point charge (taken to be a negative electron charge) at that point, minus the singular term, associated with the Coulomb potential at that point.[22,53] The numerical value of the singular term was defined as the difference between the numerical solution of eq 3.2 and the analytical electrostatic potential (obtained by the method of images) when the negative charge was located at a specific reference point, (0.5, 0.5, 0). In the numerical solution, artificial periodic boundary conditions were applied in the lateral (x, y) directions, leading to deviations of the numerical solution from the analytical one. However, as the lateral box length increases (Figure 3), the error in the numerical results decreases as expected. We emphasize here that the electrostatic potential in Figure 3 is obtained for ideal metals, whose response to the charges is described by the image charges model. This model is valid only when the charges are sufficiently far away from the metal.[54−56]

In the second model, the boundary surfaces were shaped as two electrode tips pointing toward two positive point charges. The boundary surfaces were defined as

$$z_L(x, y) = \begin{cases} \sqrt{x^2 + y^2} \le W; & -\dfrac{Z_0}{2} e^{\alpha(x^2+y^2)} \\ \sqrt{x^2 + y^2} > W; & -\dfrac{Z_1}{2} \end{cases} \tag{4.6a}$$

$$z_R(x, y) = -z_L(x, y) \tag{4.6b}$$

with the following parameters: $Z_0 = 8$ au is the minimal distance between the tips, $W = 5$ au is the radius of the tip base, $Z_1 = 18$ is the distance between the tip bases, and $\alpha = 0.03244$ au is the tip curvature parameter. The boundary electrostatic potentials were taken as

$$\Phi_L[x, y, z_L(x, y)] = 0 \qquad \Phi_R[x, y, z_R(x, y)] = 0.2 \text{ au} \tag{4.7}$$

corresponding to an electrostatic potential bias of 5.44 eV between the two electrodes. Two proton charges were located at points (0, 0, −2) and (0, 0, 2) au on the grid. In the lateral directions (x and y), periodic boundary conditions were applied as in the first model. The numerical grid parameters are reported in Table 1. In Figure 4 , contour plots of 2D sections through the solution to Poisson's equation are given for this system. Some details of the convergence of the numerical solution are given in Figure 5, where we follow the numerical error as the iterative solution proceeds. The numerical error was defined as the Euclidian norm of the residual vector,

$$\mathbf{R}^{(k)} = [\hat{\Delta} + \hat{B}]\Phi^{(k)} - b \tag{4.8}$$

and the numerical effort was measured in terms of the number of operations of the left-hand operator in eq 3.3. For comparison, we also plot in Figure 5 the convergence of the Krylov subspace expansion for the *original* linear system (eq 2.7). The significant reduction in the number of iterations in the preconditioned system (eq 3.3) is typical in this type of calculation, and it justifies our strategy of combining a fast separable Poisson solver for the cubic problem with an error-minimization scheme to solve the equation on the irregular domain with noncubic boundaries. The theoretical basis for the improved acceleration of the solver when an approximate inverse is applied as a preconditioner is commonly attributed to the clustering of the spectrum around unity (e.g., the application of the Fourier grid preconditioner in ref 43) and to the diminishing of the condition number. Interestingly, however, we found that in the particular example of Figure 5 improved convergence is obtained despite an increase in the condition number of the preconditioned system. A rigorous basis for the acceleration of the QMR algorithm in this case, therefore, requires a more detailed analysis of the spectral properties of the linear system.

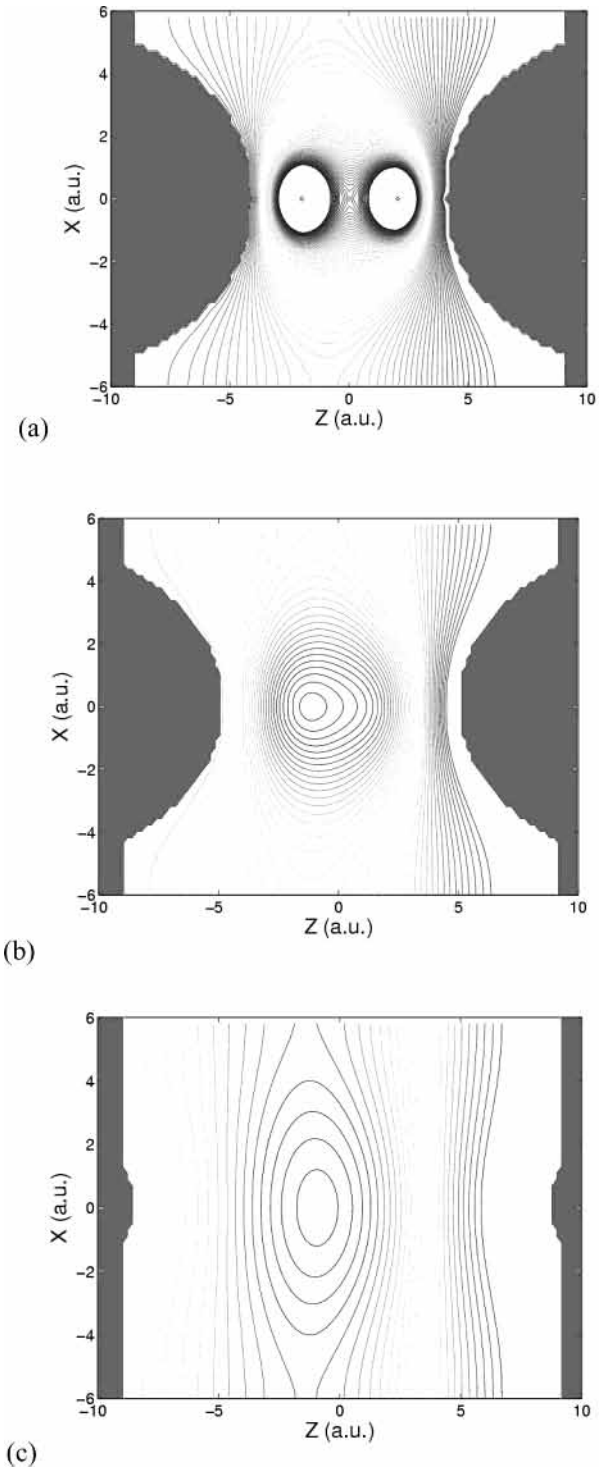

Figure 4. Contour plots of the solution to the Poisson equation for two point charges between two tips. The 2D sections in the $x-z$ plane correspond to $y = 0$, 2.4, 4.8 au from top to bottom, respectively. The dark areas are the corresponding sections through the tips.

Finally, the electrostatic potential was calculated for a negative point charge in the setup of the second model. As in the first model, the metals were considered to be ideal (macroscopic) surfaces. In Figure 6 , the z dependence of the electrostatic potential is plotted for fixed values $x = 0$ and $y = 0$ au (i.e., along the axis that passes through the positive charges). The electrostatic potential at each point was obtained as above by solving the Poisson equation numerically with the appropriate tip-shaped boundary surfaces and with an additional negative point charge. The procedure for the subtraction of the singular term from the solution of Poisson's equation at the location of the negative point charge was adopted from ref 22 (i.e., the numerical singularity at a grid point was defined in a reference electrostatic problem of two flat electrodes, as in the discussion of Figure 3). The plot in Figure 6 demonstrates the singularities associated with the positive charges as well as an attraction toward the ideal metal surfaces.

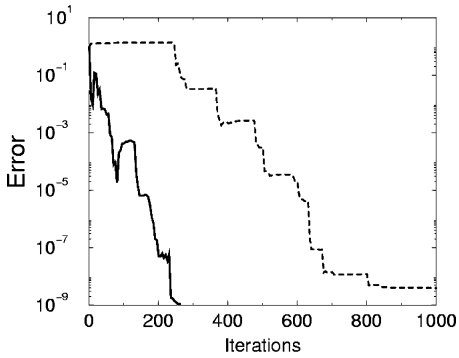

Figure 5. Typical convergence plot. The dashed and the solid lines correspond to solutions of the original (eq 2.2) and the preconditioned (eq 3.2) systems (with a constant shift of $c = 1$ au), respectively. The numerical error is defined according to eq 4.7 as the norm of the residual vector, and the numerical effort is measured in the number of operations of the left-hand operator in each equation.

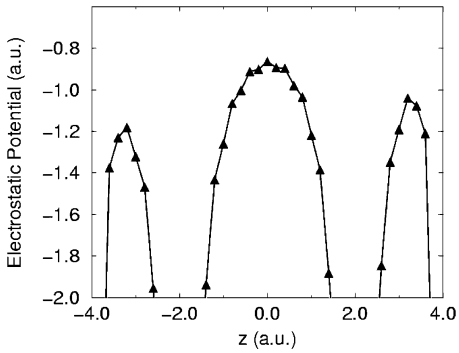

Figure 6. Numerically calculated electrostatic potential for a negative charge in a junction between two tips. Two positive charges are positioned between the tips, and an external potential bias is applied. The numerical grid parameters are given in Table 1.

5. Discussion and Conclusions

In conclusion, we have introduced a fast iterative Poisson solver for a general class of electrostatic boundary value problems on irregular, noncubic grids, which may appear in molecular junctions' geometries. We have demonstrated that the strategy of embedding the system in a cubic mesh with appropriate boundary operators is quite accurate; its convergence is fast, but mainly, its implementation is straightforward and requires an efficient FFT and a Krylov subspace-based iterative solver, which are commonly available. The price for this simplicity of implementation is that the 3D grid is expanded to contain the entire boundaries within a cubic box. However, a detailed analysis of the efficiency of our embedding method, in comparison to other more involved solvers such as domain decomposition, is beyond the scope of the present work. For the physical problem considered here (i.e., a charge distribution between two electrodes) convergence was reached within a small number of iterations even when the discretized equation was represented on large grids for improved accuracy. Given that the algorithm can be easily implemented on any complex region and efficiently implemented on massively parallel machines,[46,47,49] we anticipate that it is of valuable potential use.

The use of the Fourier basis in the present applications introduces the well-known effect of the Gibbs phenomenon at the sharp boundary interfaces (due to the discontinuous first derivative of the solution). Corrections for this problem were recently suggested[27] and can be implemented within the framework of the present algorithm. Other more simple alternatives for improved accuracy are the use of a more accurate procedure for computing the residual within the Krylov subspace accelerator.

Finally, we point out that the use of a plane wave (Fourier) basis to represent the electrostatic potential makes the result very convenient for accurate numerical integration with standard quantum chemistry basis functions, such as Gaussians. We are currently pursuing applications of the proposed Poisson solver within quantum chemical calculations for constrained molecules in metal−molecule−metal junctions.

Acknowledgment. This article is dedicated to Professor D. J. Kouri, a teacher and a friend indeed, who has demonstrated many times the usefulness of elaborate mathematical tools for the understanding of modern chemical physics. This research was supported by the Israel Science Foundation and by the fund for the promotion of research at the Technion.

References and Notes

(1) Roth, S.; Joachim, C. *Atomic and Molecular Wires*; Kluwer: Dordrecht, The Netherlands, 1997.

(2) *Molecular Electronics: Science and Technology*; Aviram, A., Ratner, M. A., Eds.; Annals of the New York Academy of Sciences 852; New York Academy of Science: New York, 1998.

(3) Bumm, L. A.; Arnold, J. J.; Cygan, M. T.; Dunbar, T. D.; Burgin, T. P.; Jones, L., II; Allara, D. L.; Tour, J. M.; Weiss, P. S. *Science* **1996**, *271*, 1705.

(4) Reed, M. A.; Zhou, C.; Muller, C. J.; Burgin, T. P.; Tour, J. M. *Science* **1997**, *278*, 252.

(5) Kergueris, C.; Bourgoin, J.-P.; Palacin, S.; Esteve, D.; Urbina, C.; Magoga, M.; Joachim, C. *Phys. Rev. B* **1999**, *59*, 12505.

(6) Reichert, J.; Ochs, R.; Beckmann, D.; Weber, H. B.; Mayor, M.; Lohneysen, H. v. *Phys. Rev. Lett.* **2002**, *88*, 176804.

(7) Weber, H. B.; Reichert, J.; Weigend, F.; Ochs, R.; Beckmann, D.; Mayor, M.; Ahlrichs, R.; Lohneysen, H. v. *Chem. Phys.* **2002**, *281*, 113.

(8) Smit, R. H. M.; Noat, Y.; Untiedt, C.; Lang, N. D.; van Hemert, M. C.; van Ruitenbeek, J. M. *Nature* **2002**, *419*, 906.

(9) Di Ventra, M.; Lang, N. D.; Pantelides, S. T. *Chem. Phys.* **2002**, *281*, 189.

(10) Derosa, P. A.; Seminario, J. M. *J. Phys. Chem. B* **2001**, *105*, 471.

(11) Taylor, J.; Guo, H.; Wang, J. *Phys. Rev. B* **2001**, *63*, 245407.

(12) Xue, Y.; Datta, S.; Ratner, M. A. *Chem. Phys.* **2002**, *281*, 151.

(13) Damble, P.; Ghosh, A. W.; Datta, S. *Phys. Rev. B.* **2002**, *64*, 201403.

(14) Alavi, S.; Larade, B.; Taylor, J.; Guo, H.; Seideman, T. *Chem. Phys.* **2002**, *281*, 293.

(15) Heurich, J.; Cuevas, J. C.; Wenzel, W.; Schon, G. *Phys. Rev. Lett.* **2002**, *88*, 256803.

(16) Baer, R.; Neuhauser, D. *Int. J. Quantum Chem.* **2003**, *91*, 524.

(17) Becke, A. D.; Dickson, R. M. *J. Chem. Phys.* **1988**, *89*, 2993.

(18) Pan, L.-H.; Sullivan, T. E.; Peridier, V. J.; Cutler, P. H.; Miskovsky, N. M. *Appl. Phys. Lett.* **1994**, *65*, 2151.

(19) Mujica, V.; Roitberg, A. E.; Ratner, M. *J. Chem. Phys.* **2000**, *112*, 6834.

(20) Lang, N. D.; Avouris, P. *Phys. Rev. Lett.* **2000**, *84*, 358.

(21) Nitzan, A.; Galperin, M.; Ingold, G.-L.; Grabert, H. *J. Chem. Phys.* **2002**, *117*, 10837.

(22) Galperin, M.; Toledo, S.; Nitzan, A. *J. Chem. Phys.* **2002**, *117*, 10817.

(23) Pleutin, S.; Grabert, H.; Ingold, G.-L.; Nitzan, A. *J. Chem. Phys.* **2003**, *118*, 3756.

(24) Buzbee, B. L.; Golub, G. H.; Nielson, C. W. *SIAM J. Numer. Anal.* **1970**, *7*, 627−656.

(25) Dorr, F. W. *SIAM Rev.* **1970**, *12*, 248−263.

(26) Hockney, R. W. *J. ACM* **1965**, *12*, 95−113.

(27) Braverman, E.; Israeli, M.; Averbuch, A.; Vozovoi, L. *J. Comput. Phys.* **1998**, *144*, 109−136.

(28) Buneman, O. SUIPR report 294; Stanford University: Stanford, CA, 1969.

(29) Swarztrauber, P. N.; Sweet, R. A. *TOMS* **1979**, *5*, 352−364.

(30) Morgan Pickering *An Introduction to Fast Fourier Transform Methods for Partial Differential Equations, with Applications*; Research Studies Press: Letchworth, England, 1986.

(31) Smith, G. D. *Numerical Solution of Partial Differential Equations: Finite Difference Methods*; Oxford University Press: New York, 1986.

(32) Ciarlet, P. G. *The Finite Element Method for Elliptic Problems*; *SIAM* **2002**.

(33) Trottenberg, U.; Osterlee, C.; Schuller, A. *Multigrid*; Academic Press: New York, 2000.

(34) Smith, B.; Bjorstad, P.; Gropp, *W. Domain Decomposition: Parallel Multilevel Methods for Elliptic Partial Differential Equations*; Cambridge University Press: New York, 1996.

(35) Freund, R. W.; Golub, G. H.; Nachtigal, N. *Acta Numer. 1* **1992**.

(36) Saad, Y. *Iterative Methods for Sparse Linear Systems*; PWS: Boston, 1996.

(37) Buzbee, B. L.; Dorr, F. W.; George, J. A.; Golub, G. H. *SIAM J. Numer. Anal* **1971**, *8*, 722−736.

(38) O'Leary, D. P.; Widlund, O. *Math. Comp.* **1979**, *33*, 849−879.

(39) McKenney, A.; Greengard, L.; Mayo, A. *J. Comput. Phys.* **1995**, *18*, 348−355.

(40) Freund, R. W.; Nachtigal, N. *Numer. Math.* **1991**, *60*, 315.

(41) Freund, R. W. *SIAM J. Sci. Comput.* **1993**, *14*, 470.

(42) Freund, R. W.; Nachtigal, N. *QMRPACK* and applications; ORNL Technical Report (ORNL/TM-12753, 1994). Freund, R. W.; Nachtigal, N. *QMRPACK*: A package of QMR algorithms; *ACM Trans. Math. Software* **1996**, *22*, 46.

(43) Peskin, U.; Edlund, A.; Miller, W. H. *J. Chem. Phys.* **1995**, *103*, 10030−10041.

(44) Edlund, A.; Vorobeichik, I.; Peskin, U. *J. Comput. Phys.* **1997**, *138*, 788−800.

(45) Vorobeichik, I.; Moiseyev, N.; Neuhauser, D.; Orenstein, M.; Peskin, U. *IEEE J. Quantum Electron.* **1997**, *33*, 1236−1244.

(46) Edlund, A.; Peskin, U. *Int. J. Quantum Chem.* **1998**, *69*, 167−173.

(47) Edlund, A.; Bar-On, I.; Peskin, U. *Applied Parallel Computing*; Kagstrom, B., Dongarra, J., Elmroth, E., Wasniewski, J., Eds.; Lecture Notes in Computer Science 1541; Springer-Verlag: Berlin, 1998; pp 112−119.

(48) Peskin, U.; Edlund, A.; Bar-On, I.; Galperin, M.; Nitzan, A. *J. Chem. Phys.* **1999**, *111*, 7558−7566.

(49) Bar-On, I.; Edlund, A.; Peskin, U. *Appl. Numer. Math.* **2000**, *33*, 95−104.

(50) Poirier, B.; Carrington, T. J., Jr. *Chem. Phys.* **2001**, *114*, 9254−9264.

(51) Poirier, B.; Carrington, T., Jr. *J. Chem. Phys.* **2002**, *116*, 1215−1227.

(52) Nielsen, I. M. B.; Janssen, C. L. *Comput. Phys. Commun.* **2001**, *136*, 29.

(53) Jackson, J. D. *Classical Electrodynamics*; Wiley: New York, 1999.

(54) Nordlander, P.; Tully, J. C. *Phys. Rev. Lett.* **1988**, *61*, 990.

(55) Nordlander, P.; Tully, J. C. *Phys. Rev. B* **1990**, *42*, 5564.

(56) Deutscher, S. A.; Yang, X.; Burgdorfer, J. *Phys. Rev. A* **1997**, *55*, 466.